Biosensors and Bioelectronics ■ (■■■■) ■■■–■■■

Contents lists available at ScienceDirect

Biosensors and Bioelectronics

journal homepage: www.elsevier.com/locate/bios

AuNPs modified, disposable, ITO based biosensor: Early diagnosis of heat shock protein 70

Münteha Nur Sonuç Karaboğa [a], Çiğdem Sayıklı Şimşek [b], Mustafa Kemal Sezgintürk [b,*]

[a] Namık Kemal University, School of Health, Nutrition and Dietetics Department, Tekirdağ, Turkey
[b] Namık Kemal University, Faculty of Science and Arts, Chemistry Department, Biochemistry Division, Tekirdağ, Turkey

ARTICLE INFO

Article history:
Received 23 June 2015
Received in revised form
19 August 2015
Accepted 20 August 2015

Keywords:
Heat shock proteins
HSP70
ITO
Gold nanoparticles
Immunosensor

ABSTRACT

This paper describes a novel, simple, and disposable immunosensor based on indium-tin oxide (ITO) sheets modified with gold nanoparticles to sensitively analyze heat shock protein 70 (HSP70), a potential biomarker that could be evaluated in diagnosis of some carcinomas. Disposable ITO coated Polyethylene terephthalate (PET) electrodes were used and modified with gold nanoparticles in order to construct the biosensors. Optimization and characterization steps were analyzed by electrochemical techniques such as electrochemical impedance spectroscopy (EIS) and cyclic voltammetry (CV). Surface morphology of the biosensor was also identified by electrochemical methods, scanning electron microscopy (SEM), and atomic force microscopy (AFM). To interpret binding characterization of HSP70 to anti-HSP70 single frequency impedance method was successfully operated. Moreover, the proposed HSP70 immunosensor acquired good stability, repeatability, and reproducibility. Ultimately, proposed biosensor was introduced to real human serum samples to determine HSP70 sensitively and accurately.

1. Introduction

Heat shock proteins are defined as molecular chaperones and they play an important role in the cellular stress response including heat, toxicants, reactive oxygen species, injuries, diseases, and other stressors (Jego et al., 2013). They can be classified into five super families according to their molecular weights: small HSPs, HSP40, HSP70, HSP90, and HSP110. Several gene families encode them, the HSP70 family is found in response to stress in all organisms as conserved form (Pyza et al., 1997; Seigneuric et al., 2011). HSP70 attends to a large variety of folding processes including folding of newly synthesized proteins, refolding of misfolded proteins and control of the activity of regulatory proteins (Hartl and Hayer-Hartl, 2002; Mayer and Bukau, 2005; Young et al., 2003). HSP70 could be a remarkable biomarker because its overexpression in serum is associated with many cancers. Recently, a research group determined HSP70 by Enzyme-Linked Immonosorbent Assay (ELISA) and they showed the presence of this potential biomarker in the plasma of mice carrying human xenograft tumors (Gehrmann et al., 2014). Moreover, the plasma HSP70 levels are connected with the amount of tumor localized in mice tissue relevant to the potential of HSP70 as predictive tumor marker. High expression of this chaperone molecule informs about increased tumor grade and poor prognosis as well (Calderwood et al., 2006; Ciocca and Calderwood, 2005; Murphy, 2013). For instance, HSP70 overexpression is a potential marker of early stage of hepatocellular and prostate cancer (Abe et al., 2004; Chuma et al., 2003), breast cancer (Lazaris et al., 1997), lymph node metastasis in colorectal carcinoma (Hwang et al., 2003), bladder urothelial carcinoma (Garg et al., 2010), pancreatic cancer (Dutta et al., 2012). Besides, levels of HSP70 in serum can be correlated to proliferation and tumor size in uterine cervical cancer (Ralhan and Kaur, 1995).

The small sizes of gold nanoparticles are mostly used in electrochemical based biosensors applications due to their stable chemical and physical properties. More importantly they present great stable surface for further immobilization process activity that can be evaluated in biosensor systems. Moreover gold nanoparticles provide many advantages such as enhancing surface width, their capability to minimalize the space between proteins and metal particles, and to form a pathway that conducts electrons between redox proteins and the electrode surfaces (Shipway et al., 2000; Yanez-Sedeno and Pingarron, 2005).

Recently the applications of indium tin oxide (ITO) film electrodes have increased interest in biosensor fabrications owing to their high electrical conductivities, excellent substrate affinity, wide range electrochemical working area, stable electrochemical and physical properties and also very low costs although it has disposable properties (Lin et al., 2007).

* Corresponding author.
E-mail addresses: msezginturk@hotmail.com, msezginturk@nku.edu.tr (M.K. Sezgintürk).

http://dx.doi.org/10.1016/j.bios.2015.08.044
0956-5663/

In our previous studies 3-aminopropyltriethoxysilane (APTES) have been attached on the activated ITO surface for the immobilization of biomolecules (Canbaz and Sezgintürk, 2014; Şimşek et al., 2014). In the current study, gold nanoparticles were chosen as the conductive material to modify ITO electrode in order to enhance the electrical characteristics of ITO substrate. Anti-HSP70 antibody was covalently immobilized with the help of cysteamine, which introduced a self-assembled monolayer on the gold nanoparticles modified ITO surface. To evaluate immobilization steps of the immunosensor cyclic voltammetry (CV) and electrochemical impedance spectroscopy (EIS) techniques were employed. Scanning electron microscopy (SEM) and atomic force microscopy (AFM) techniques were performed for the characterization of surface morphology of the biosensors as well. Current optimization experiments were done for the fabrication of the biosensor carrying optimal requirements. Repeatability and reproducibility parameters were also examined. The applicability of the proposed biosensor was very important, consequently several real human serum samples were analyzed by our biosensor and these results were successively confirmed by a standard method. Lastly, in order to monitor interaction between HSP70 and anti-HSP70 immobilized onto gold nanoparticles modified ITO electrode surface, an effective impedimetric technique namely single frequency impedance was practised as well.

2. Materials and methods

ITO-coated PET films (The transmittance and surface resistivity are 550 nm (> 79%) and 60 Ω/square, respectively) and the other reagents were supplied from Sigma-Aldrich (St. Louis, MO, USA). Phosphate buffer system (50 mM, pH 7.0) were used to prepare anti HSP70, HSP70 and 1% bovine serum albumin (BSA) solutions which were stored at −20 °C until use. Phosphate buffer that comprised 1 M KCl, 5 mM $[Fe(CN)_6]^{4-}$ and 5 mM $[Fe(CN)_6]^{3-}$ was applied as a redox probe solution in all electrochemical experiments. The real samples were obtained by research ethics committee approval with the number of 2013/86/07/05 from Namık Kemal University, Faculty of Medicine. Gamry Potentiostate/Galvanostate, Reference 600 interfaced with a PC via EChem Analyst program was used for electrochemical experiments. A three-electrode system that consisted of a sheet of ITO substrate (2 mm × 20 mm) as a working electrode and, a silver/silver chloride reference electrode, and a Pt wire counter electrode was performed in the experimental system.

2.1. Fabrication of the anti HSP70 based impidimetric biosensors

Cleaning procedure of ITO substrates was the first step of the building up the biosensor. The ITO substrates were polished by sonicated in acetone, soap solution and ultra distilled water respectively for 10 min. Before use, electrodes were dried under an ultra pure stream of argon.

2.2. Preparation of gold nanoparticles

Before AuNP preparation, all glassware was cleaned by aqua regia solution, which was consisting of mixing 3 volumes hydrochloric acid (HCl) to 1 volume nitric acid (HNO_3). In order to obtain 500 mL of 0.2 mM gold nanoparticles, 1 mL amount of 0.1 M $HAuCl_4$ aqueous solution was transferred to the 500 mL of distilled water. 500 mL of 10 mL 0.13 M sodium borohydride ($NaBH_4$) was added dropwise to the 500 mL of solution containing $HAuCl_4 \cdot 3H_2O$ while stirring. The color of the solution should change from yellow to ruby red (Kah et al., 2008; Low and Bansal, 2010). Then, cleaned ITO-PET electrodes were immersed in this solution for 24 h in a dark ambient. After this, the electrodes were washed with ultra-pure water and dried with argon gas gently.

2.3. Covalent immobilization of anti-HSP70 onto SAMs of cysteamine

In the following step, gold nanoparticle modified ITO-PET electrodes were instantly immersed in a cysteamine solution (60 mM in pure ethanol) and left them overnight in the dark. Later, they were rinsed with ethanol and distilled water respectively and then dried by a pure argon stream. For the covalent interaction between SAMs of cysteamine on AuNP modified ITO electrodes and anti HSP70, glutaraldehyde solution of 0.1% was used as cross-linking agent for 15 min. Then, ITO electrodes were immersed into 100 μL of antiHSP70 solution in a dark medium. After that ITO electrodes were washed with distilled water to remove physically bound biomolecules, and then dried with argon gas gently. Finally, the electrodes were immersed in BSA solution (1%) to block the active glutaraldehyde ends on the electrode surface. A representative scheme explaining the modification and assembly of ITO based biosensor was presented in Supplemental Scheme 1.

2.4. Electrochemical characterization

Cyclic voltammetry and electrochemical impedance measurements were performed to characterize the steps of electrode modification and immobilization. All electrochemical measurements (CV and EIS) were performed in 5 mM $K_3[Fe(CN)_6]/K_4[Fe(CN)_6]$ (1:1) solution which served as a redox probe containing 0.1 M KCl (Şimşek et al., 2014).

Morphological observation of the different surfaces obtained when the fabrication process of the biosensor, a field emission scanning electron microscope (FEI-Quanta FEG 250) was operated at the Scientific and Technological Research Center of Namık Kemal University (NABILTEM). 5 kV was used as an acceleration voltage to obtain SEM images. Moreover atomic force microscopy images were also used in the evaluation of the different modification steps. For this purpose an atomic force microscope (Nanomagnetic Instruments, Turkey) was used at the Scientific and Technological Research Center of Namık Kemal University (NABILTEM) as well.

2.5. Testing principle

After each of the ITO-based biosensors was assembled, the biosensor surface was used to interact with the HSP70 solution. The electrode was immersed into the standard solution of HSP70. The response value was read after one-hour incubation in this standard solution of HSP70. After this incubation period, the biosensor was gently immersed into the ultrapure water 20 times to remove physically adsorbed HSP70 molecules. Finally, the working electrode based on ITO was again put into the cell containing the $Fe(CN)_6^{4-/3-}$ redox probe solution and the electrochemical measurements were carried out as described previously. HSP70 calibration curves were constructed by using impedance variations before and after incubations carried out in the HSP70 standard solutions.

3. Results and discussion

3.1. Immobilization of anti-HSP70 onto ITO substrate

The first step of the anti-HSP70 immobilization was to form SAMs of cysteamine onto the gold nanoparticle modified ITO electrode surface. By reason of having high surface free energy and wide specific surface area, gold nanoparticles can adsorb

Please cite this article as: Sonuç Karaboğa, M.N., et al., Biosensors and Bioelectronics (2015), http://dx.doi.org/10.1016/j.bios.2015.08.044

biomolecules lustily during immobilization process of biosensor fabrication. When the biomolecules are adsorbed to naked surface of ITO material directly, they can lose their bioactivity. On the other hand, biomolecules which are adsorbed onto the surface modified by nanoparticles can keep their activity owing to biocompatibility of gold nanoparticles (Luo et al., 2006). Consequently in this study, using gold nanoparticles were very important because of two reasons; one was the gold nanoparticles enhanced the biocompatibility of ITO sheets and the second one was the gold nanoparticles effectively increased the conductivity of ITO surface.

Cysteamine is a short chain molecule, which has thiol groups bound to colloidal gold surface strongly. Then, glutaraldehyde was used as a cross-linking agent that binds amine groups found on cysteamine and the other amino ends at the antibody molecules. Glutaraldehyde is a popular homo-bifunctional agent, specifically reacting with primary amine groups and can form strong inter- and intra-molecular covalent bonds. In the presented immobilization procedure, glutaraldehyde played a role of crosslinker between the amino ends of cysteamine and the primary amino groups of anti-HSP-70. BSA was used as a blocking agent during the biosensor fabrication to prevent non-specific binding on the electrode surface after anti-HSP70 immobilization. All of these steps are summarized in Supplemental information Scheme 1.

The step-by-step construction of biosensor was characterised by electrochemical techniques, CV and EIS. $K_3[Fe(CN)_6]/K_4[Fe(CN)_6]$ couple is used as electron transferring mediator that can significantly participate in the redox reaction with the biological component and the electrode surface and in this way, supports to the rapid electron transfer.

EIS has been performed to monitor both the building of biosensors and the biosensor's recognition process. This powerful method supplied significant information about all steps of fabrication of the working electrode and its optimization experiments. The impedance spectra of each immobilization step of the anti-HSP70 are displayed in Fig. 1.A. A typical impedance spectrum is presented in the form of the Nyquist plot (Fig. 1.A) that consists of two sections; a semicircle part at higher frequencies meaning to the electron-transfer limited process and a linear portion at lower frequency range corresponding to the diffusion-limited process. The semicircle diameter in an impedance spectrum indicates the electron transfer resistance; R_{ct}. Electron-transfer kinetics of the redox probe at the electrode-solution interface is controlled by electron transfer resistance. The charge transfer resistance (R_{ct}) value of bare ITO was assessed to be 32,720 Ω, which was reduced to 5670 Ω after the gold nanoparticles physically adsorbed onto bare ITO electrodes, which represented significant electron transfer kinetics between the redox couple and the electrode surface interface associated to the adsorption of gold nanoparticles. However, when the ITO/AuNP electrode was layered by cysteamine, charge-transfer resistance again decreased significantly implying the formation of amino group of cysteamine. These amino ends founded as protonated at that pH (pKa=8.27) which might provide the negatively charged redox probe to diffuse onto the electrode surface easily. Following that, the R_{ct} value of the ITO/AuNP/cysteamine electrode was increased clearly after anti-HSP70 was immobilized onto the ITO surface. This also proved the formation of anti-HSP70 layer on the modified ITO electrode surface successfully, which showed a blocking effect to the electron transfer kinetics. Final step of immobilization procedure was to inhibit active glutaraldehyde ends by BSA solution also caused a further increase in the electron transfer resistance.

A well-defined characteristic voltammogram of the redox couple could be observed from Fig. 1.B., which agreed well with the impedance spectra results. The formation of cysteamine SAM

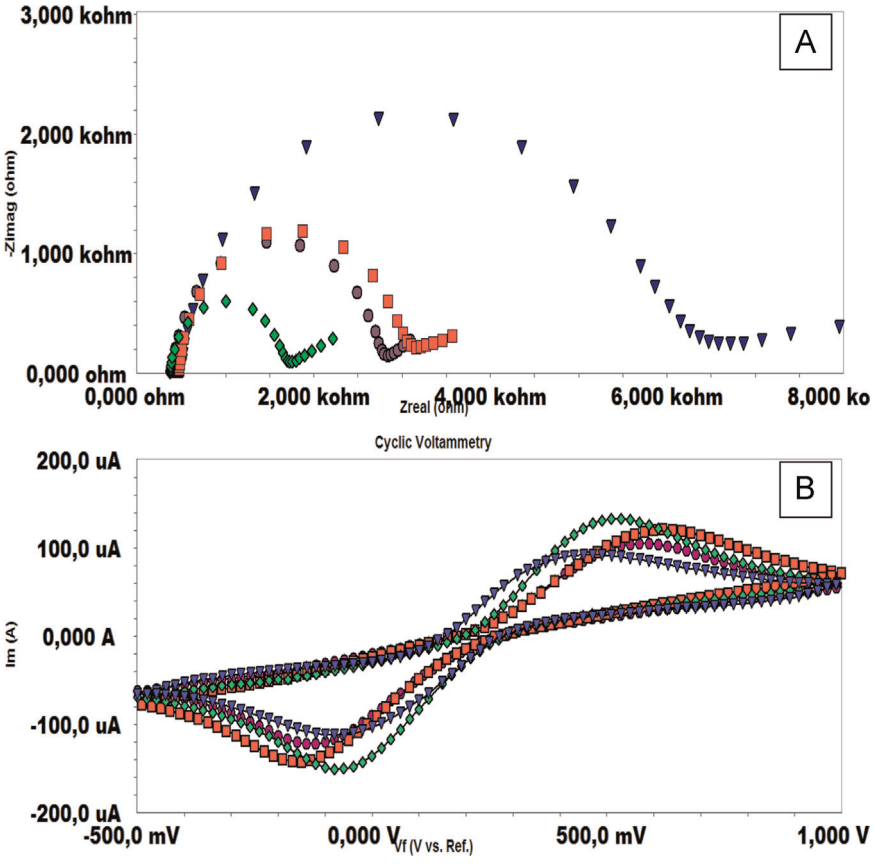

Fig. 1. Electrochemical impedance spectra **(A)** and cyclic voltammograms **(B)** corresponding to anti-HSP70 immobilization steps [-▾-▾-: ITO/AuNP, -◆-◆-: ITO/AuNP/cysteamine, - ●-●-: ITO/AuNP/cysteamine/anti-HSP70, -■-■-: ITO/AuNP/cysteamine/anti-HSP70/BSA].

Please cite this article as: Sonuç Karaboğa, M.N., et al., Biosensors and Bioelectronics (2015), http://dx.doi.org/10.1016/j.bios.2015.08.044

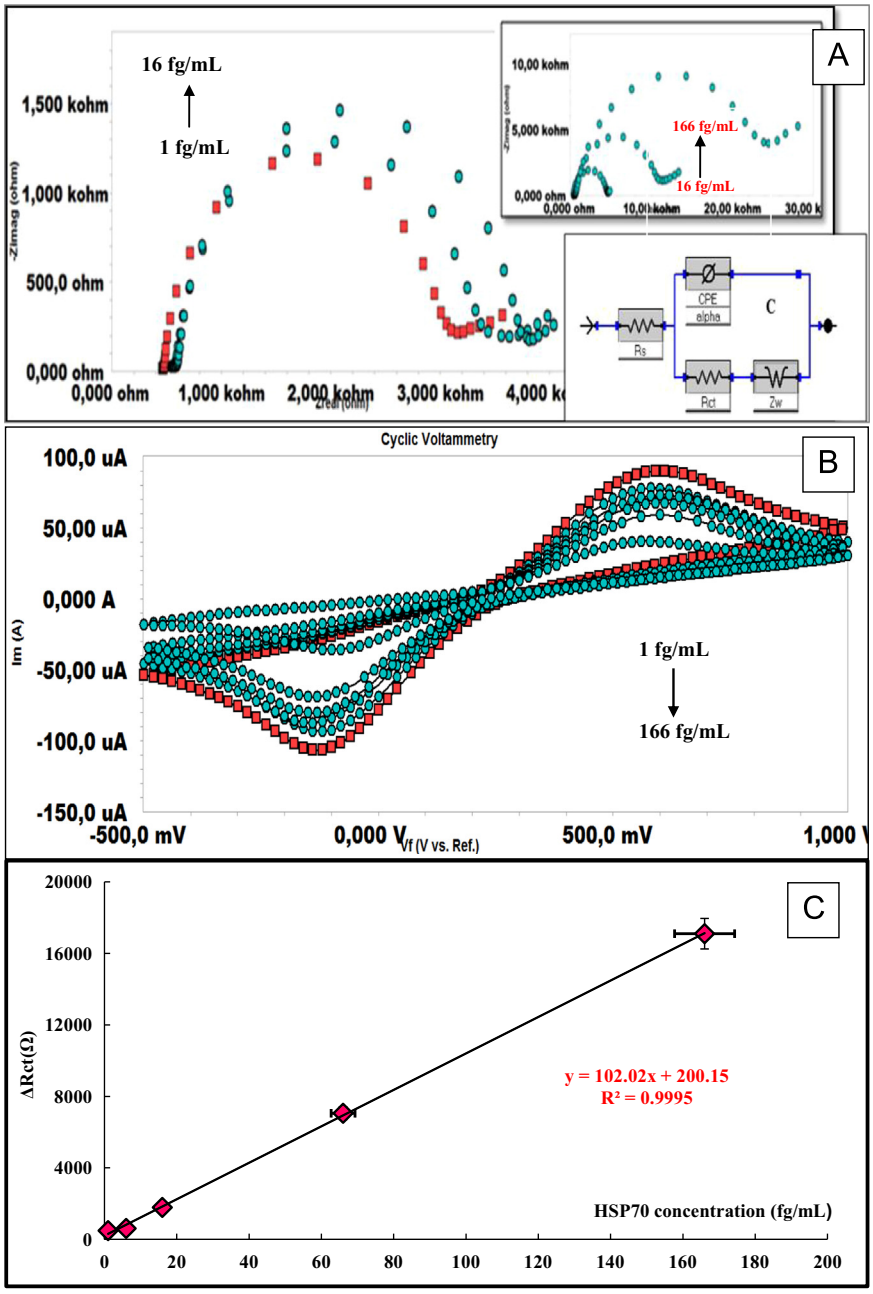

Fig. 2. Impedance spectra **(A)**, cyclic voltammograms **(B)** obtained for different concentrations of HSP70, and HSP70 calibration curve **(C)** obtained by the biosensor based on anti-HSP70 at optimal working conditions. In the inset equivalent circuit model was applied to fit the impedance measurements. In this model R_s represents ohmic resistance of electrolyte solution; C_{dl} is associated with double layer capacitance; R_{et} corresponds electron transfer resistance, and W is Warburg impedance.

on the ITO surface resulted in an apparent increase in anodic and cathodic currents compared with the peak currents of gold nanoparticle modified ITO surfaces. Formation of the cysteamine monolayer on ITO electrode modified with gold nanoparticle caused an increase in the faradic currents due to electrostatic attraction between positively charged cysteamine monolayer and negatively charged redox probe. After covalent attachment of anti-HSP70, both the cathodic and the anodic peak currents were decreased considerably due to the barrier effect of anti-HSP70 on the electron transfer rate. Glutaraldehyde, a much-used cross linking agent, has been used in a variety of applications where maintenance of structural rigidity of protein is important and can react with some functional groups of proteins, included, thiol, phenol, amine, and imidazole because nucleophiles which are localized on amino acid side-chains are very reactive. Finally the addition of BSA that blocked free active ends also caused a further decrease in peak currents due to its insulator protein structure.

3.2. Optimization studies of HSP70 biosensor

In the optimization studies of the anti-HSP70 based biosensor, some of the experimental parameters such as antibody concentration and antibody incubation time were investigated to obtain a sensitive, repeatable, and reproducible biosensor system.

To clarify the influence of anti-HSP70 concentration on the response of biosensor system, 1–166 fg/mL of HSP70 standard solutions were determined by the biosensor system designed with different concentrations of anti-HSP70 (0.25, 0.5, 1.0, 2.0 and 8.0 μg/mL). As seen from calibration curves (Supplemental information Fig. 1) differences in concentration of anti-HSP70

Table 1
Comparison of methods developed for HSP70, artificial serum and real human serum sample analyses.

Comparison of current developed methods for HSP70 determination

Methods	Measurement principle	Detection range	References
ELISA	Commercial kit	0.20–12.5 ng/mL	Cui et al. (2015)
ELISA	Commercial kit	780–50,000 pg/mL	Njemini et al. (2005)
LSPR	Label free SPR	0.92–4000 ng/mL	Denomme (2012)
SPR	Magnetic microbeads based SPR	0.3–30 μg/mL	Sun et al. (2007)
Piezoelectric sensor	Biomimetic peptides	60–200 nM	Mascini et al. (2006)

HSP70 detection in artificial serum samples (fg/mL HSP70)

Added	Found by the biosensor	% Recovery	% Relative difference
5	4.97	99.4	0.6

Real human serum sample experiments (fg/mL HSP70)

Sample	Found by the biosensor	Added HSP70 amount	Total found	% Recovery	% Relative difference
1	4.64	5	9.54	98.8	1.2
2	3.11	5	7.96	98.2	1.8
3	3.76	5	8.51	97.1	2.9
4	4.06	5	8.83	97.5	2.5
5	6.75	5	11.22	95.5	5.5

reflected to both the peak currents (CV) and electron transfer resistance (EIS) values. Levels of anti-HSP70 concentration lower than 1.0 μg/mL were not adequate to obtain sensitive and valid biosensor signals. By reason of low concentration of anti-HSP70 on the electrode surface did not allow binding HSP70 successfully.

On the other hand, high concentrations of anti-HSP70 provided high R_{ct} values owing to thick protein layer occurring on the electrode surface. Moreover high concentrations of anti HSP70 might cause a destruction of the well-organized of the surface due to random protein–protein interactions and consequently the linearity of response was diverged as seen from the Supplemental information Fig. 1. According to the response linearity and maximum R_{ct} values, 1 μg/mL anti-HSP70 was determined as the optimum concentration for appropriate biosensor construction.

The next optimization parameter was the incubation period of anti-HSP70 to determine the most effective binding period for the covalent immobilization of anti-HSP70. For this purpose, modified working electrodes were incubated into the anti-HSP70 solutions for different periods as 30, 60, 75 and 90 min. From the results, the incubation period of anti-HSP70 affected the biosensor response substantially. The results are shown as HSP70 calibration graphs with different incubation period of anti-HSP70 in Supplemental information Fig. 2. R^2 values related to incubation periods of 30, 60, 75, and 90 min were calculated as 0.2793, 0.9578, 0.9802, and 0.7374 respectively. As seen from the graph and R^2 values, a period of 30 min was obviously not enough for the effective immobilization of anti-HSP70. Beside, 90 min of incubation period might damage the electrode surface and therefore only 3 different concentrations of HSP70 could be analyzed by the biosensor that was fabricated by using 90 min incubation period. This damage probably caused from the high protein amount on the electrode surface and its densely formed bioactive layer which also gave rise to high insulating effect on the surface. Although R^2 values of 60 min and 75 min were close to each other, R_{ct} values of 75 min was significantly higher than 60 min. As a consequence, 75 min incubation period of antiHSP70 was chosen as optimal incubation period of anti-HSP70 for the further studies.

3.3. Analytical characteristics of the biosensor

After the optimization studies, the constructed biosensor was characterised according to its linear range, repeatability and reproducibility. To acquire a linear relation between HSP70 concentrations and charge transfer resistance the absolute impedance values were extracted from the impedance spectra by using an electrical equivalent circuit model inserted into Fig. 2.A.

In this model, R_s refers to the resistance of the electrolyte solution, CPE shows the double layer capacitance of the system, Z_w is the Warburg element, and R_{ct} indicates the charge transfer resistance in the low frequency range. Following equation was used to calculate the impedance change that was used in HSP70 calibration graph, $\Delta R_{ct} = R_{ctHSP70} - R_{ctBSA}$.

Nyquist plots of the fabricated biosensor for different HSP70 concentrations (1.0, 6.0, 16, 66, 166 fg/mL) are demonstrated in Fig. 2.A. When HSP70 concentration increased, semicircle diameter in the Nyquist plot was also increased proportionally. This increase was linear in the range of HSP70 concentrations from 1 fg/mL to 166 fg/mL. This result revealed that the new biosensor had a fairly wide determination range for HSP70 and could allow analyzing HSP70, sensitively and accurately.

Correlatively, CV peak currents decreased with an increased in the concentration of HSP70 standard solutions (Fig. 2.B). This was also an expected result because high amount of HSP70 on the surface introduced a high insulating barrier for the diffusion of the redox probe to the electrode surface. Linear calibration graph of HSP70 was drawn by means of the changes in R_{ct} after HSP70 applications and it is given in Fig. 2.C.

As mentioned earlier, the linear detection range obtained by the presented biosensing system represents more sensitive measurement system than some commercial immunoassay methods, which are used routinely, and other biosensor based techniques such as surface plasmon resonance. A comparison of these systems should be seen in Table 1.

For example a SPR biosensor system via magnetic microbeads to determine HSP70 was developed. This system was operated in the different determination ranges depend on different dilution ratios of the conjugates (Sun et al., 2007). In other system, a limit of detection (LOD) for HSP70 concentration has also been reported as 0.0620 fg/mL which was lower than HSP70 level of healthy human serum (Molvarec et al., 2007).

To calculate LOD and LOQ (limit of quantification) following equations were used: $[k^*S_{blank}/m]$. In this simple equation, k is a constant, which is accepted as 3 and 10 in LOD and LOQ calculations, respectively. S_{blank} and m represent the signal of blank sample and the slope, respectively. LOD and LOQ values were determined as 0.0618 fg/mL and 0.206 fg/mL, respectively. LOD and LOQ results are showed that the present biosensor could successfully be operated in sensitive detection of HSP70.

The repeatability of AuNP based ITO biosensor signals was determined by analysis of the same concentration of HSP70 (16 fg/mL) with the electrodes that were prepared under the similar conditions. It was found out that the immunosensor had an excellent repeatability bearing in mind that the correlation coefficient of the analysis was 5.85% and the average value and standard deviation were calculated as 16.4 fg/mL and 0.96 fg/mL, respectively.

The reproducibility of the new antiHSP70 immunosensor was

also experienced by using of 13 biosensors constructed via the same set of procedures. As specified by the results achieved, the biosensor presented here had satisfactory reproducible properties. The linear detection of 12 biosensors for HSP70 was the same between 1–166 fg/mL. The relative standard deviations (RSD) were also calculated for the slopes and the intercepts of the resulting linear equations as 5.6% and 4.9%, respectively. As a conclusion the repeatability and the reproducibility of the new biosensing system were fairly good and showed acceptable analytical results for the detection of HSP70.

Usually, Kramers–Kronig transforms appear very sensitive criteria of the validity of the AC impedance data (Sezgintürk, 2011; Sonuç and Sezgintürk, 2014). To estimate data quality and accuracy, the Kramers–Kronig (K–K) relations can be used. Integration of the imaginary part and vice versa was acquired by the real part of an impedance spectrum. In the current study, via Kramers–Kronig Transforms an imaginary part of a linear, stable, and causal circuit was calculated by the real part of the experimental data obtained. Likewise, the imaginary portion of the experimental data was used to calculate the real part of a stable, linear, and causal circuit. By this calculation, "Goodness of Fit" values were also procured (Asav and Sezgintürk, 2014; Şimşek et al., 2015). Goodness of fit values can be seen in Supplemental information Table 1.

An acceptable "goodness of fit" value has to be around 1. If this value is close to 1, probably the model calculated fits well with the experimental impedance data. Contrary to this, higher values than 1 should mean that the model calculated does not fit the experimental data. Moreover in some circumstances, the goodness of fit value should be obtained as lower than 1 that should be attributed to the error limits have probably been set too large (Flannery et al., 1992).

3.4. Single frequency impedance (SFI) experiments

To characterize the binding HSP70 to anti-HSP70, single frequency impedance technique was used as well. SFI method can be operated in protein–protein, DNA–protein, or any interactions like among the biomolecules to identify the important kinetic parameters. With this method, at a fixed frequency value, electrochemical impedance can be measured versus time. For this aim, the potentiostate was set up at a fixed frequency of 1 Hz. This value was selected by evaluating the Bode plots, which contained important frequency information related with the system. However Nyquist diagrams have not frequency data and have simple connection to the electrical model. In other respects Bode plots comprise all the required information (Macdonald and Barsoukov 2005). Hence Bode plots are primarily applied in the circuit analysis. The impedance was measured at the fixed frequency as a function of time and phase angle for 60 min. As it is seen from Fig. 3, single frequency impedance data introduced remarkable facts about the binding of HSP70 to anti-HSP70.

In the figure, time-dependent change of impedance was presented by green curve while the change in the phase angle as a function time was showed by pink curve. As a result of the interaction between anti-HSP70 and HSP70, 227 Ω and 1.76° were found as the changes in the charge transfer resistance and phase angle, respectively. During this experiment, although the measurements were taken in a Faraday cage, all the systems including the potentiostate were isolated as far as possible from any electromagnetic waves or inductive effects possibly caused from the environment. Consequently, from the results it should be stated that the single frequency impedance could effectively be used in biosensor researches and to monitor time dependent binding characteristics of biological molecules onto the biosensor surface.

To investigate the short shelf life of the fabricated biosensor, the immunosensors were stored at 4 °C for periods 5 and 15 days.

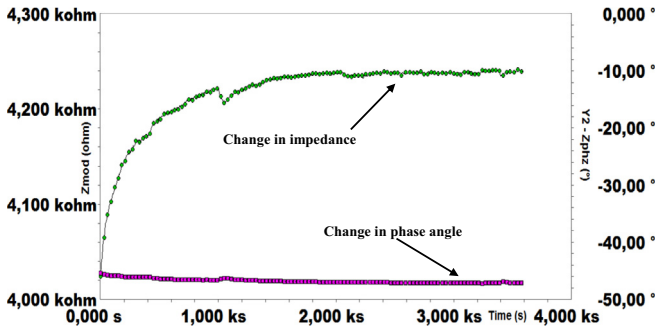

Fig. 3. Single frequency impedance experiment [-●-●-: variations in the impedance value, -■-■-: variations in the phase angle. This experiment was carried out at a fixed frequency of 1 Hz versus time (60 min), 227 Ω and 1.76° were found as the changes in the charge transfer resistance and phase angle after the interaction between anti-HSP70 and HS70].

The biosensor responses were stable for the 15 days. The present biosensor retained its stability 92.29% at the end of 15th day.

3.5. SEM and AFM observations

SEM and AFM techniques give appreciable information about biosensor surface layer by layer. By this means morphological characteristics of constructed biosensor are also observed significantly.

Fig. 4.1.A illustrates a SEM image of an ITO electrode surface after modification with gold nanoparticles. It can be seen that the diameters of gold nanoparticles were measured in the range of 50–80 nm. Fig. 4.1.B shows biosensor surface modified by SAMs of cysteamine. The picture should be distinguished by its cloudy appearance especially on the gold nanoparticles. When anti-HSP70 was immobilized on the electrode surface, cotton wool spots appeared on the modified surface, which could be attributed to the anti-HSP70 molecules (Fig. 4.1.C). After BSA attachment, as a blocking protein, globular big spots were observed on the surface (Fig. 4.1.D). In consequence of interaction between anti-HSP70 and HSP70, a densely ordered and spongelike formation was attributed to the binding of HSP70 molecules to the electrode surface (Fig. 4.1. E).

The influence of anti-HSP70 immobilization on the topology of ITO surface was also evaluated by AFM experiments. Firstly gold nanoparticles modified ITO surface was scanned with the AFM in tapping mode in air. In the AFM pictures given in Fig. 4.2, the dark areas represent flat of ITO surface and bright areas represent elevated areas on the ITO surfaces as molecular interactions occur. Starting with this information, gold nano particles can be seen in Fig. 4.2.A as little knaps overspreaded on ITO surface. After, cysteamine SAM formed onto gold nanoparticles should clearly be distinguished by the help of densely layered appearance of the molecules in Fig. 4.2.B. Covalently attachment of anti-HSP70 onto the ITO surface considerably affected the surface topology (Fig. 4.2. C). After anti-HSP70 immobilization, the little knaps observed previously were disappeared and instead of this the surface topology looked like a desert caused from protein molecules. Finally, because BSA molecules were larger than anti-HSP70 molecules, after BSA modification, appearance of the elevated areas on the ITO surface was an expected topological change (Fig. 4.2.D).

Finally, the new gold nanoparticle based biosensor was assayed for artificial and real human serum samples to detect HSP70 level. For this purpose, real serum samples were first diluted for 10^5 times because an HSP70 content of healthy person serum is extremely higher than the linear detection range of the proposed biosensor. The result of these experiments can be found in Table 1 in which a comparison between the results of hospital analyses

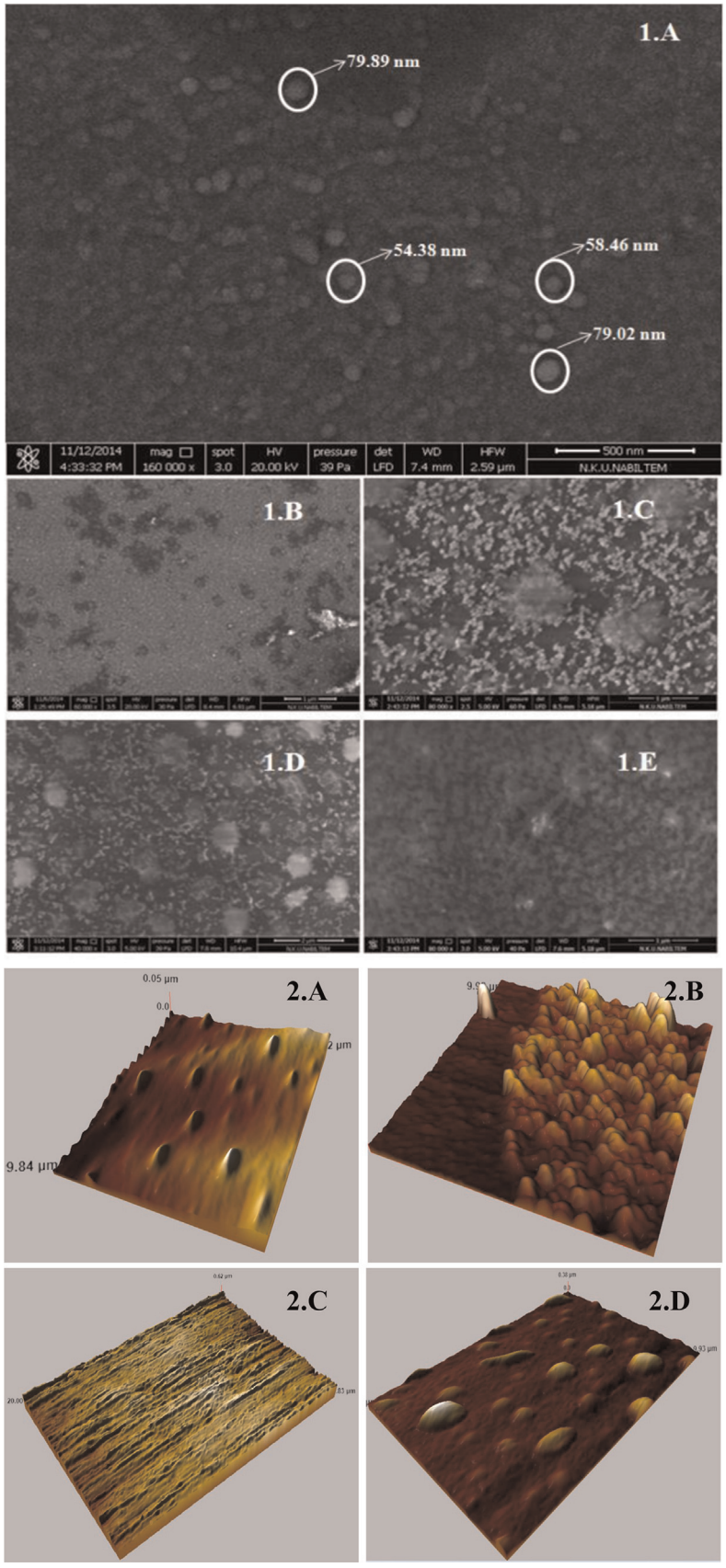

Fig. 4. SEM and AFM pictures related with the morphological variations during the immobilization steps of the new biosensor based on AuNPs modified ITO electrodes [SEM figures: **1.A** – ITO/AuNP, **1.B** – ITO/AuNP/cysteamine, **1.C –** ITO/AuNP/cysteamine/Anti-HSP70, **1.D –** ITO/AuNP/cysteamine/ Anti-HSP70/BSA, **1.E** – ITO/AuNP/cysteamine/Anti-HSP70/BSA/HSP70][AFM figures: **2.A** – ITO/ AuNP, **2.B** – ITO/AuNP/cysteamine, **2.C –** ITO/AuNP/cysteamine/Anti-HSP70, **2.D –** ITO/AuNP/ cysteamine/Anti-HSP70/BSA].

Please cite this article as: Sonuç Karaboğa, M.N., et al., Biosensors and Bioelectronics (2015), http://dx.doi.org/10.1016/j.bios.2015.08.044

and the presented new biosensor could also be found. As seen from the results, the presented biosensor system was able to determine HSP70 in real human serum samples with sensitively and accurately.

4. Conclusion

In the current study, we present a novel biosensor which has simple immobilization procedure by gold nanoparticles and self-assembled monolayers of cysteamine to sensitively detect HSP70 in human serum samples. ITO based disposable biosensing system provides sensitively and accurately detection of HSP70. The real human serum and artificial serum sample experiments showed that there was no undesirable interference effects of other species to the biosensor surface. Consequently, it can be concluded that the ITO material should support to prevent undesirable physical boundings to the surface by the help of its structural characteristics such as the hydrophobic feature of its surface which, should not introduce any weak interactions with the hydrophilic outer surface of any protein. Using gold nanoparticles both enhances the electrical conductivity of ITO and also introduces an effective immobilization possibility in conjunction with cysteamine SAM. Moreover relatively good storage stability can be attributed to using stable cysteamine SAM on the ITO surface. Moreover, binding kinetics of HSP70 to antiHSP70 is simultaneously monitored by single frequency technique. A wide determination range for HSP70 (1–166 fg/mL), well repeatability and reproducibility, and low cost fabrication of ITO based electrodes are the most important superiorities of the new biosensing system reported here. Beside it must definitely be emphasized that this biosensor system is disposable and should be seen as the most promising candidate for the development of point-of-care biosensing systems for other biologically important compounds. All steps of biosensor construction were characterized by CV and EIS supporting by SEM and AFM images as well. Shelf life of the present biosensor system for relatively short terms is good, although for further studies it has to be tried to evaluate the long shelf life of the biosensor, which is especially a significance in clinical applications before general use. Finally, this new biosensor system can detect HSP70 level in human serum samples sensitively and accurately.

Acknowledgment

The financial support from TÜBİTAK (The Scientific and Technological Research Council of Turkey, Project number: 113 Z 678) is gratefully acknowledged.

Appendix A. Supplementary material

Supplementary data associated with this article can be found in the online version at http://dx.doi.org/10.1016/j.bios.2015.08.044.

References

Abe, M., Manola, J.B., Oh, W.K., Parslow, D.L., George, D.J., Austin, C.L., Kantoff, P.W., 2004. Clin. Prostate Cancer 3 (1), 49–53.
Asav, E., Sezgintürk, M.K., 2014. Int. J. Biol. Macromol. 66, 273–280.
Calderwood, S.K., Khaleque, M.A., Sawyer, D.B., Ciocca, D.R., 2006. Trends Biochem. Sci. 31 (3), 164–172.
Canbaz, M.Ç., Sezgintürk, M.K., 2014. Anal. Biochem. 446, 9–18.
Chuma, M., Sakamoto, M., Yamazaki, K., Ohta, T., Ohki, M., Asaka, M., Hirohashi, S., 2003. Hepatology 37 (1), 198–207.
Ciocca, D.R., Calderwood, S.K., 2005. Cell Stress Chaperones 10 (2), 86.
Cui, X., Xing, J., Liu, Y., Zhou, Y., Luo, X., Zhang, Z., Han, W., Wu, T., Chen, W., 2015. Cell Stress Chaperones 20 (3), 473–481.
Denomme, R., 2012. A Label-free Biosensor for Heat Shock Protein 70 Using Localized Surface Plasmon Resonance.
Dutta, S.K., Girotra, M., Singla, M., Dutta, A., Stephen, F.O., Nair, P.P., Merchant, N.B., 2012. Pancreas 41 (4), 530.
Flannery, B.P., Teukolsky, S., Vettering, W.T., 1992. Numerical Recipes, second edition. W.H. Press, Cambridge.
Garg, M., Kanojia, D., Seth, A., Kumar, R., Gupta, A., Surolia, A., Suri, A., 2010. Eur. J. Cancer 46 (1), 207–215.
Gehrmann, M., Specht, H.M., Bayer, C., Brandstetter, M., Chizzali, B., Duma, M., Breuninger, S., Hube, K., Lehnerer, S., van Phi, V., 2014. Radiat. Oncol. 9 (131), 717–719.
Hartl, F.U., Hayer-Hartl, M., 2002. Science 295 (5561), 1852–1858.
Hwang, T.S., Han, H.S., Choi, H.K., Lee, Y.J., Kim, Y.J., Han, M.Y., Park, Y.M., 2003. J. Gastroenterol. Hepatol. 18 (6), 690–700.
Jego, G., Hazoumé, A., Seigneuric, R., Garrido, C., 2013. Cancer Lett. 332 (2), 275–285.
Kah, J., Olivo, M., Lee, C., Sheppard, C., 2008. Mol. Cell Probes 22 (1), 14–23.
Lazaris, A.C., Chatzigianni, E.B., Panoussopoulos, D., Tzimas, G.N., Davaris, P.S., Golematis, B.C., 1997. Breast Cancer Res. Treat. 43 (1), 43–51.
Lin, J., Qu, W., Zhang, S., 2007. Anal. Biochem. 360 (2), 288–293.
Low, A., Bansal, V., 2010. Biomed. Imaging Interv. J. 6 (1), e9.
Luo, X., Morrin, A., Killard, A.J., Smyth, M.R., 2006. Electroanalysis 18 (4), 319–326.
Macdonald, J.R., Barsoukov, E., 2005. History 1, 8.
Mascini, M., Del Carlo, M., Compagnone, D., Cozzani, I., Tiscar, P., Mpamhanga, C., Chen, B., 2006. Anal. Lett. 39 (8), 1627–1642.
Mayer, M., Bukau, B., 2005. Cell Mol. Life Sci. 62 (6), 670–684.
Molvarec, A., Rigó, J., Nagy, B., Walentin, S., Szalay, J., Füst, G., Karádi, I., Prohászka, Z., 2007. J. Reprod. Immunol. 74 (1), 163–169.
Murphy, M.E., 2013. Carcinogenesis 34 (6), 1181–1188.
Njemini, R., Demanet, C., Mets, T., 2005. J. Immunol. Methods 306 (1), 176–182.
Pyza, E., Mak, P., Kramarz, P., Laskowski, R., 1997. Ecotoxicol. Environ. Safe 38 (3), 244–251.
Ralhan, R., Kaur, J., 1995. Clin. Cancer Res. 1 (10), 1217–1222.
Seigneuric, R., Mjahed, H., Gobbo, J., Joly, A.-L., Berthenet, K., Shirley, S., Garrido, C., 2011. Front. Oncol. 1 (37), 1–10.
Sezgintürk, M.K., 2011. Biosens. Bioelectron. 26, 4032–4039.
Shipway, A.N., Katz, E., Willner, I., 2000. Chemphyschem 1 (1), 18–52.
Sonuç, N.M., Sezgintürk, M.K., 2014. Talanta 120, 355–361.
Sun, Y., Bai, Y., Song, D., Li, X., Wang, L., Zhang, H., 2007. Biosens. Bioelectron. 23 (4), 473–478.
Şimşek, Ç.S., Teke, M., Sezgintürk, M.K., 2014. Electroanalysis 26 (2), 328–339.
Şimşek, Ç.S., Karaboğa, M.N.S., Sezgintürk, M.K., 2015. Talanta 144, 210–218.
Yanez-Sedeno, P., Pingarron, J., 2005. Anal. Bioanal. Chem. 382 (4), 884–886.
Young, J.C., Barral, J.M., Hartl, F.U., 2003. Trends Biochem. Sci. 28 (10), 541–547.

Please cite this article as: Sonuç Karaboğa, M.N., et al., Biosensors and Bioelectronics (2015), http://dx.doi.org/10.1016/j.bios.2015.08.044